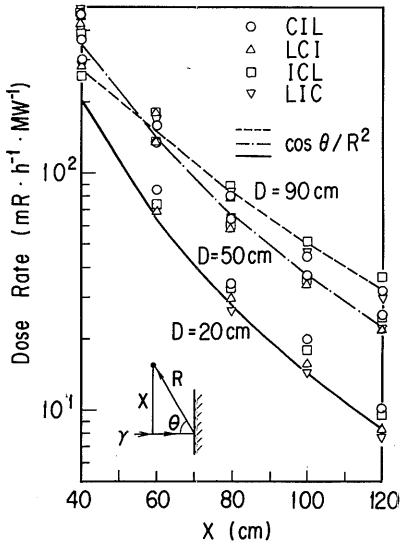

Fig. 20 X-directional dose rate distributions measured in front of the shield.

Dose rates in front of the shield are determined by the components (3), (4), and (5). The contribution of the component (4) can be approximately estimated with the measurement for the configuration of which no shield in the cavity and the rear door is open. In this territory, the main contribution of the component (5) is considered due to the gamma rays penetrating through the shield and then reflected at the rear wall. This contribution can be estimated with the difference of doses measured in the two configurations in which no shield in the cavity with the rear door open or closed. This amount resulted in negligible small at measurement positions in front of the shield. Thus, dose rates corresponding to the component (3) were obtained by eliminating only the contribution of the component (4) from measured dose rates. They are shown in Figs. 21-23 by comparing with calculations based on the above formula.

Since the first slabs of the CIL and ICL arrangement are thick enough from the point of view of albedo, calculations using the albedos of concrete and iron can be considered corresponding to the measurements for the CIL and ICL arrangement, respectively. Actually, these calculations agree well with measurements except X-40 cm for D = 90 cm where the component (4) is probably included in measured values. Large differences are seen between the measurements for the LCI and LIC arrangement and the calculations using the albedo of lead. It may be said that underestimations occur at reflection angles less than about 82 deg. where experimental results are close to calculations for concrete or iron which is the second layer of the LCI or

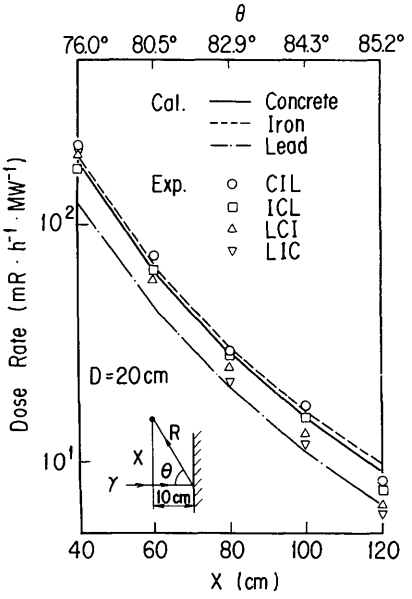

Fig. 21 Comparison of measured and calculated X-directional dose rate distributions in front of the shield placed 20 cm from the front wall.

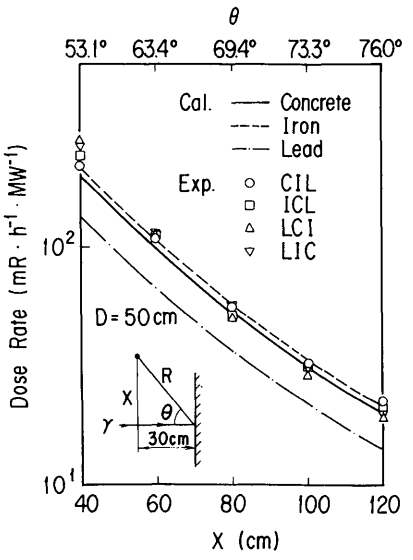

Fig. 22 Comparison of measured and calculated X-directional dose rate distributions in front of the shield placed 50 cm from the front wall.

LIC arrangement. The front lead slab in the LCI or LIC arrangement is 2.5 cm in thickness which is too thin to calculate the reflection from the LCI or LIC shield using the albedo of lead. Therefore, the effect of the second layer must be included in the calculations for the LCI or LIC arrangement. Good agreement is seen at reflection angles above about 82 deg., that is, $X > 60$ cm for $D = 20$ cm. This is probably due to large slant paths in lead at large reflection angles. For example, the slant path in lead is 15.1 cm at 80.5 deg. and increases to 20.2 cm at 82.9 deg. Thus, the 2.4 deg. increase of reflection angle turn out the 5.1 cm increase of the slant path, and experimental results become closer to the calculated values rapidly.

From these analysis, it can be concluded that the dose rate distribution in the region of $X > 40$ cm in front of shield is determined mainly by gamma rays reflected from the front surface of the shield. In this experiment, the streaming component due to multi-scattering between the front wall and the shield is not a main component. Good agreement between calculations and measurements indicates that Chilton and Huddreston's data are accurate enough to use them in this type of simple calculations.

Dose rate distributions on the line $X = 120$ cm for six CIL arrangements are shown in Fig. 24. In the figure, a peak is found that seems to move from

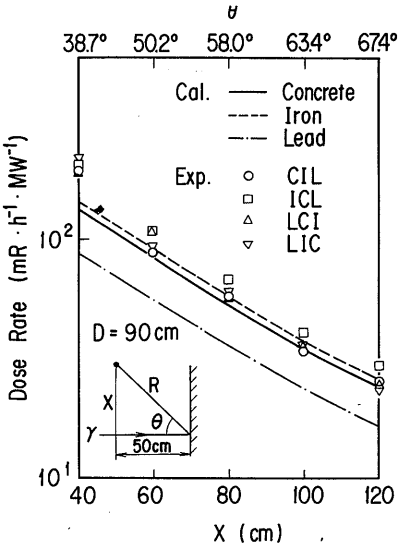

Fig. 23 Comparison of measured and calculated X-directional dose rate distributions in front of the shield placed 90 cm from the front wall.

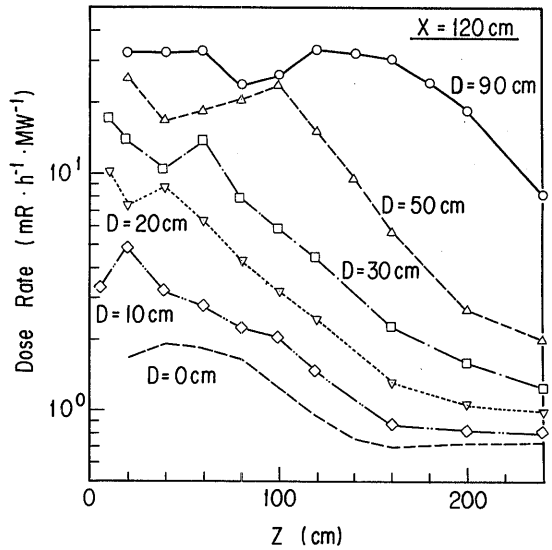

Fig. 24 Dose rate distributions measured on the traverse X = 120 cm in CIL configurations in which the shield is placed D cm from the front wall.

the incident hole to the slant direction. This is the component (4) which plays important role in the calculation described in the next chapter.

4. CALCULATIONS

For two CIL configurations having the gap width D = 50 or 90 cm, calculations were carried out using the PALLAS two-dimensional discrete ordinates transport code[9] and the MORSE Monte Carlo code.[10] PALLAS calculations in two-dimensional RZ geometries were performed for the case of D = 50 cm only. A geometrical model taken in calculations is shown in Fig. 25. The origin of the coordinates was taken at the core center where a point source was placed. R-directional dimensions of the shield and the concrete cavity were determined so as to conserve actual geometrical cross sections. Thus, a cylindrical shield with a radius of 56 cm was placed in a cylindrical cavity with a radius of 147 cm. The front wall and three iron slabs were replaced by a 35-cm-thick concrete wall to keep the length of the lead lining of the incident hole, since it was found, through calculations, that the gamma rays reflected at the lead lining play important role in the determination of dose rate distributions in the cavity.

To express the R-directional distribution of incident gamma rays, two types of absorbers were placed at the location corresponding to the outlet of

the experimental hole as shown in Fig. 25. The outer absorber is a "black" one which absorbs all gamma rays incident on it and the inner absorber is a "gray" one which absorbs only 36 percent of gamma rays incident on it. These two absorbers reproduced the radial distribution of the incident gamma rays fairly well as shown in Fig. 26 with dotted lines.

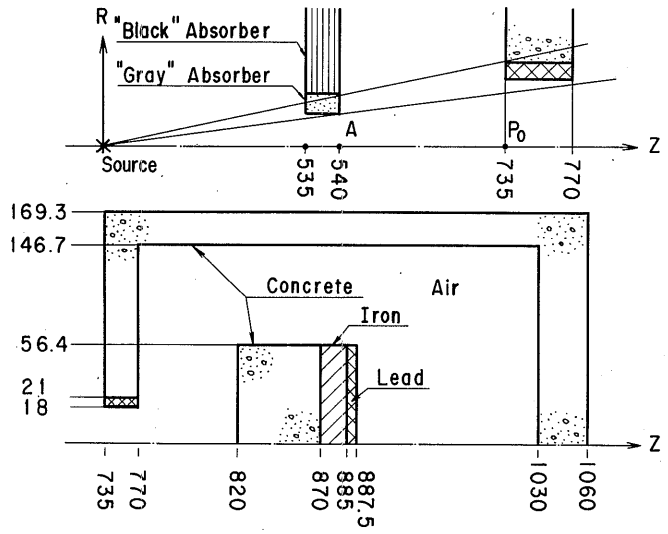

Fig. 25 Geometrical model used in PALLAS calculations. Dimensions are in centimetres.

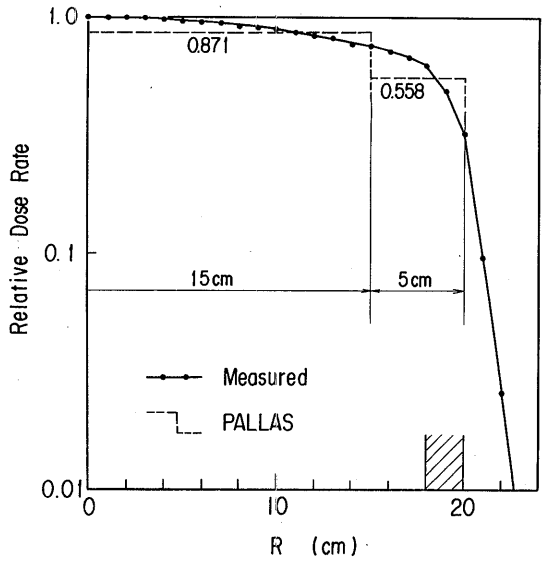

Fig. 26 X-directional dose rate distribution reproduced in PALLAS calculations.

Calculations were carried out from 8.25 MeV to 92 keV with 30 energy mesh points and with 28 angular mesh points taken on a hemisphere of which polar angles are given in Table 26. Comparisons of measured and calculated dose rate distributions on Z-directional traverses are shown in Figs. 27 and 28. Good agreement is found in front of the shield except on a line of X = 20 cm where a steep gradient of dose rates is seen in the X-direction. Good agreement is also seen behind the shield. However, large inconsistencies are found in the side air region of the shield. There are unrealistic peaks in the calculations. It seems that a peak moves from the incident hole to the direction corresponding to the angle θ_3 in Table 26. Therefore it was expected that this is due to the ray-effect arising from inaccurate treatment of the gamma rays scattered at the incident hole.

If this inference is true, this problem will be solved by calculating uncollided gamma rays from the incident hole analytically. Then, calculations

Table 26. Polar Angles of the Angular Quadrature Set Used in PALLAS Calculations

i	θ_i (deg.)
1	7.068
2	24.253
3	50.318
4	77.338

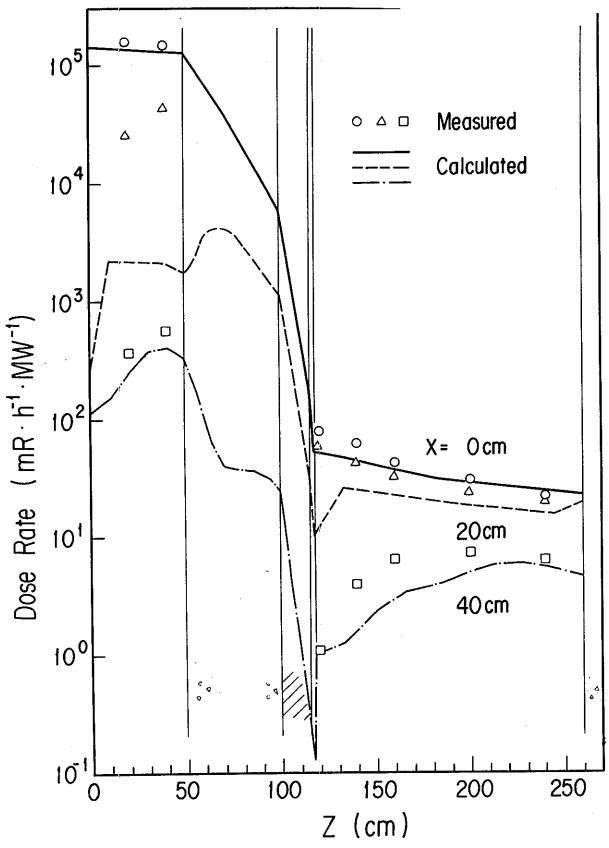

Fig. 27 Comparison of measured and calculated dose rate distributions on Z-directional traverses in the CIL configuration of D = 50 cm.

were divided geometrically into two steps. In the first step, calculations were carried out from the source to the inner surface of the front wall. In the second step, the boundary fluxes obtained by the first calculations were treated as the source from which uncollided gamma rays were calculated analytically. As shown in Fig. 29, an improvement is seen in calculated results. Therefore, the above inference on the ray-effect is acceptable and the method applied in the second calculations is effective to improve the calculational accuracy.

In these calculations, incident gamma rays were divided into two components, that is, one entering into the cavity without interacting with the materials of the front wall and the other mainly scattered at the incident hole. Dose rate distributions due to the two components are shown in Fig. 30, which indicates that the scattered gamma rays at the inner surface of the incident hole play important role in the determination of the dose rates on the traverse of X = 60 cm. Consequently, it is quite important to pay attension to the scattered gamma rays at the duct outlet in this kind of problem.

Monte Carlo calculations were carried out for two CIL configurations of

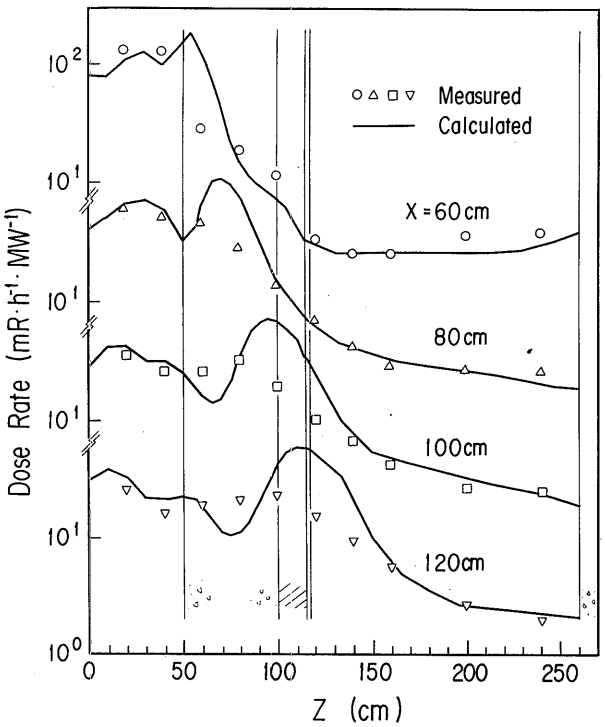

Fig. 28 Comparison of measured and calculated dose rate distribution on Z-directional traverses in the CIL configuration of D = 50 cm.

D = 50 cm and 90 cm. Accurate geometrical models were taken. Incident gamma rays were emitted from a disk source of 40 cm in diameter placed at the position P_o. They were sampled uniformly in a cone having an opening angle of 5 deg. around the axis. The radial distribution of measured incident gamma rays was accurately reproduced in calculations. The DLC-23 cross section file was used, so that P_3 calculations were carried out with 18 energy groups of which boundary energies are given in Table 27. The number of histories were chosen so that fractional standard deviations would be less than 0.1, which resulted in about five thousands.

Comparisons of measured and calculated results in front of and behind the shield are shown in Fig. 31 for D = 50 cm and Fig. 32 for D = 90 cm. Fairly good agreement is found in these areas except on the line X = 20 cm where extremely steep gradient of dose rates are seen. Comparisons of measured and calculated results in the side of the shield are shown in Fig. 33 for D = 50 cm and Fig. 34 for D = 90 cm. In spite of fairly good agreement seen in the case of D = 50 cm, rather large disagreements are found in the case of D = 90 cm. As a cause of these disagreements, inaccurate treatment

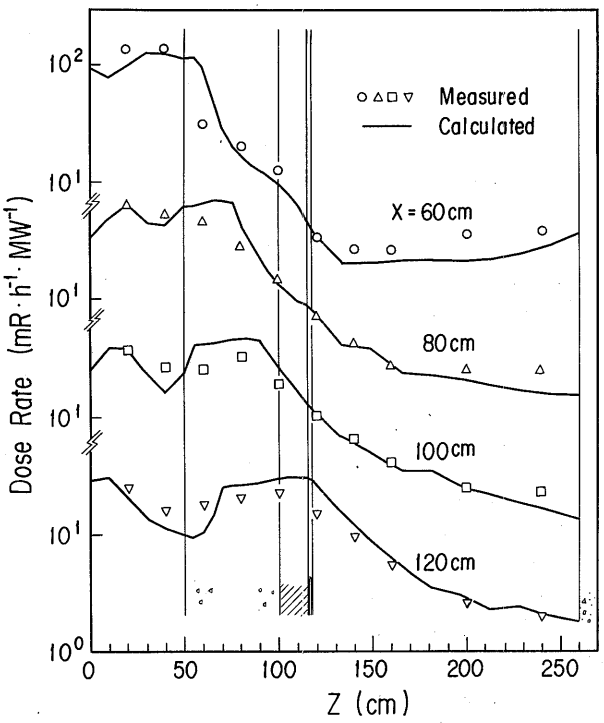

Fig. 29 Comparison of measured and calculated dose rate distributions on Z-directional traverses. Uncollided fluxes are calculated analytically.

of photon scattering with P_3 cross sections is considered. In these figures, only fractional standard deviations larger than 0.2 are indicated.

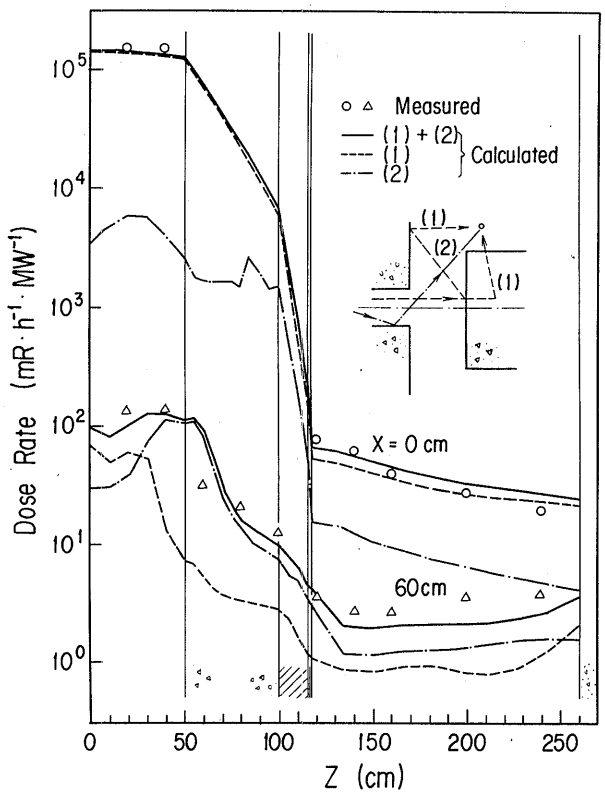

Fig. 30 Calculated dose rate distributions due to the two components of incident gamma rays.

Table 27. Energy Group Structure of MORSE Calculations

Group No.	Energy Range (MeV)	Group No.	Energy Range (MeV)
1	1.00 + 01[a] — 8.00 + 00	10	1.33 + 00 — 1.00 + 00
2	8.00 + 00 — 6.50 + 00	11	1.00 + 00 — 8.00 - 01
3	6.50 + 00 — 5.00 + 00	12	8.00 - 01 — 6.00 - 01
4	5.00 + 00 — 4.00 + 00	13	6.00 - 01 — 4.00 - 01
5	4.00 + 00 — 3.00 + 00	14	4.00 - 01 — 3.00 - 01
6	3.00 + 00 — 2.50 + 00	15	3.00 - 01 — 2.00 - 01
7	2.50 + 00 — 2.00 + 00	16	2.00 - 01 — 1.00 - 01
8	2.00 + 00 — 1.66 + 00	17	1.00 - 01 — 5.00 - 02
9	1.66 + 00 — 1.33 + 00	18	5.00 - 02 — 1.00 - 04

[a] Read as 1.00×10^1

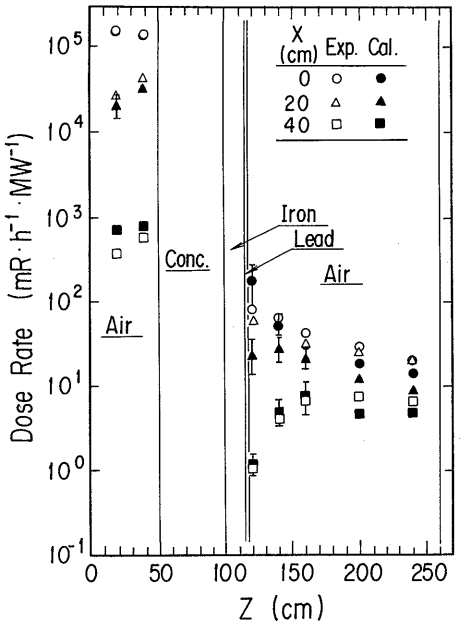

Fig. 31 Comparison of measured and calculated dose rate distributions on Z-directional traverses in the CIL configuration of D = 50 cm.

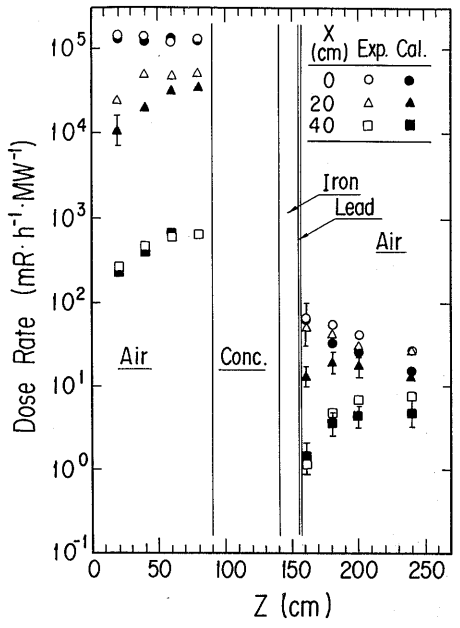

Fig. 32 Comparison of measured and calculated dose rate distributions on Z-directional traverses in the CIL configuration of D = 90 cm.

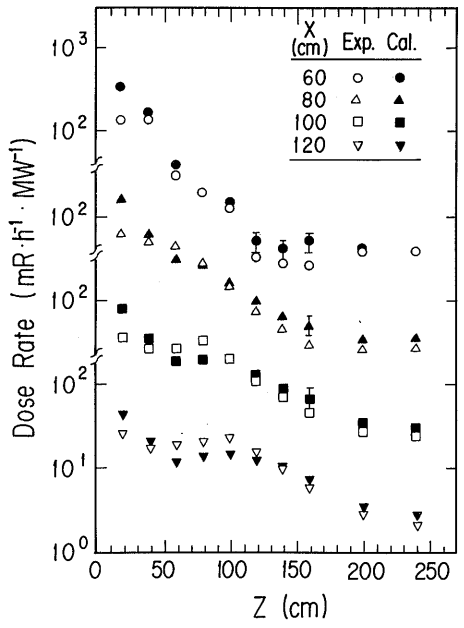

Fig. 33 Comparison of measured and calculated dose rate distributions on Z-directional traverses in the CIL configuration of D = 50 cm.

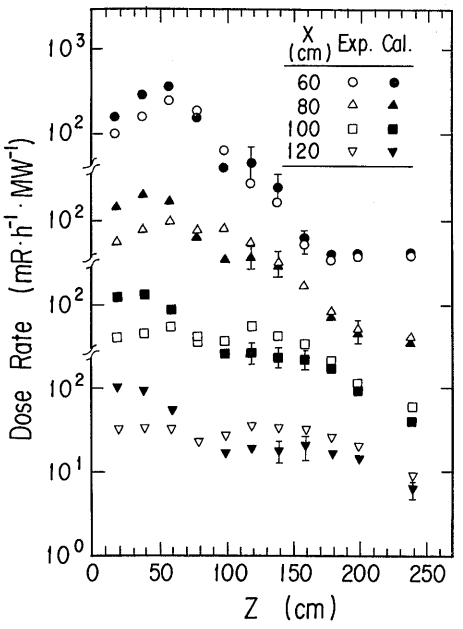

Fig. 34 Comparison of measured and calculated dose rate distributions on Z-directional traverses in the CIL configuration of D = 90 cm.

5. CONCLUSION

The following conclusions are obtained from the analysis of experimental data on the shield for leakage gamma rays from a duct.

1. For the penetration component, a better shielding effect can be obtained by setting heavier materials to the source side.
2. The same conclusion is obtained for the leakage component.
3. The reflection component can be calculated by using a simple formula and Chilton and Huddreston's albedo data.
4. The gamma rays scattered at the inside of the duct outlet play important role in the problem of additional shield.

Experimental data obtained for twenty shield configurations can be used to assess calculations of the effect of additional shields for leakage gamma rays from ducts. In calculations with the discrete ordinates transport code PALLAS, the ray-effect was found in the case of straight forward calculations because of inaccurate treatment of gamma rays scattered at the duct outlet. This problem was solved by performing analytical calculations for gamma rays scattered at the duct outlet and going to detection points without any collisions. Monte Carlo calculations with the MORSE code gave fairly good results in the configuration of D = 50 cm, however, large disagreements were found between measured and calculated results in the configuration of D = 90 cm. The cause of the disagreement was not clarified in this study, however, it was considered that one of the reasons is inaccurate treatment of photon scattering with P_3 cross sections.

ACKNOWLEDGEMENT

This work is a part of the cooperative research of the Ship Research Institute and the JAERI on the shielding of a marine reactor.

The authors wish to express their thanks to the personnel of JRR-4 for reactor operation.

REFERENCES

1) T.Miura, K. Takeuchi, and M. Kinno, Study on Additional Shields for Gamma-Rays Streaming Through a Duct, Proc. 6th Int. Conf. radiation shielding, 2, 787 (1983)
2) S. Miyasaka, A User's Manual for JRR-4 Experimental Facilities, JAERI 6016, (1965) (in Japanese)
3) K. Saito, and S. Moriuchi, Monte Carlo Calculation of Accurate Response Functions of a NaI(T1) Detector for Gamma Rays, Nucl. Instrum. Methods, 185, 299 (1981)
4) T. Miura, Assessment of Data and Methods to Form Response Functions of a 3″ϕ x 3″ NaI(T1) Detector, Nucl. Instrum. Methods, 221, 603 (1984)
5) W.R. Burrus and V.V. Verbinski, Fast Neutron Spectroscopy with Thick Organic Scintillators, Nucl. Instrum. Methods, 67, 181 (1969)
6) K. Takeuchi, S. Tanaka, and M. Kinno, Transport Calculation of Gamma Rays Including Bremsstrahlung by the Discrete Ordinates Code PALLAS, Nucl. Sci. Eng., 78, 273 (1981)
7) A.B. Chilton and C.M. Huddreston, A Semiempirical Formula for Differential Dose Albedo for Gamma Rays on Concrete, Nucl. Sci. Eng., 17, 419 (1963)
8) A.B. Chilton, C.M. Davisson, and L.A. Beach, Parameters for C-H Albedo Formula for Gamma Rays Reflected from Water, Concrete, Iron, and Lead, Trans. Am. Nucl. Soc., 8, No. 2, 656 (1965)
9) K. Takeuchi, PALLAS-2DCY-FC, A Calculational Method and Radiation Transport Code in Two-Dimensional (R, Z) Geometry, Papers Ship Res. Inst., No. 57 (1979)
10) E.A. Straker et al., The MORSE Code — A Multigroup Neutron and Gamma-Ray Monte Carlo Code, ORNL-4585, (1970)